JOURNAL OF COMPUTATIONAL PHYSICS **140,** 205–232 (1998)
ARTICLE NO. CP975887

On Performance of Methods with Third- and Fifth-Order Compact Upwind Differencing

Andrei I. Tolstykh and Michael V. Lipavskii

Computing Center of Russian Academy of Sciences, Moscow Vavilova str. 40, Russia
E-mail: tol@ccas.ru, lipav@ccas.ru

Received February 17, 1997; revised October 21, 1997

The difference schemes for fluid dynamics type of equations based on third- and fifth-order Compact Upwind Differencing (CUD) are considered. To validate their properties following from a linear analysis, calculations were carried out using the inviscid and viscous Burgers' equation as well as the compressible Navier–Stokes equation written in the conservative form for curvilinear coordinates. In the latter case, transonic cascade flow was chosen as a representative example. The performance of the CUD methods was estimated by investigating mesh convergence of the solutions and comparing with the results of second-order schemes. It is demonstrated that the oscillation-free steep gradients solutions obtained without using smoothing techniques can provide considerable increase of accuracy even when exploiting coarse meshes.

Key Words: compact upwind differencing; high-order schemes; Burgers and Navier–Stokes equations; cascade flow.

1. INTRODUCTION

In the seventies, the high-accuracy technique was proposed for fluid dynamics which was based on the third-order compact upwind differencing (CUD-3) idea [1]. In subsequent years, it was extensively used for solving various compressible and incompressible viscous flows described by the Navier–Stokes equations and their simplified forms [2]. As its extension, the fifth-order CUD (CUD-5) was described [3] and validated as a part of the $\psi - \omega$ method for incompressible flows [4].

Application of the CUD approach to viscous flows showed that high-accuracy oscillation-free solutions can be obtained for many practical cases without using any artificial smoothing devices (limiters, additional dissipation, etc.) as far as steady state solutions are concerned.

Investigations into the CUD-3 schemes for unsteady inviscid computations were initiated in [5]. They have been continued in [6], resulting in high-resolution schemes for the Euler

0021-9991/98 $25.00

equations. Applications of the CUD-3 to unsteady compressible Navier–Stokes equations were reported also in [7].

In the early nineties, new versions of the third- and fifth-order compact upwind discretizations were proposed and investigated theoretically [8, 9]. They can be referred to as CUD-II-3 and CUD-II-5. The general CUD theory and applications up to 1993 can be found in [10]. Other types of upwind compact formulas with pentadiagonal matrix operators were considered in [11, 12].

At present, it is clear how to construct formally arbitrary-order compact differencing (in general, nonsymmetric) formulas which are some rational functions of conventional difference operators [10]. However, the important point here is to choose those which lead to stable schemes, at least in the case of constant coefficients and unbounded domains (or periodic functions). However, even if theoretical studies are carried out and necessary stability proofs are presented, the question arises to what extent the resulting schemes are competitive. The question is not trivial, since it follows only from the well-known theorem "nth-order discretization + stability = nth-order convergence" that asymptotic mesh convergence order can be at least n. In fact, accuracy estimates depend also on constants characterizing the sensitivity of the numerical solutions of resulting difference systems to input data perturbations. For example, high-order centered approximations to the first derivatives can lead to ill-conditioned systems with little hope of obtaining accurate solutions. Moreover, there are some factors in many real-life problems which have the potential for neutralizing the possible advantages of high-order schemes. They are, for example, nonsmooth meshes in curvilinear coordinates, low-order discretizations of viscous terms, and computational costs when solving resulting algebraic systems.

Although considerable knowledge was obtained while solving various CFD problems with CUD-3 (and partially with CUD-5), comparatively recent approximations CUD-II-3 and CUD-II-5 were investigated mainly theoretically. Theoretical analysis [8–10] indicated that they can be especially beneficial when applied to steady-state problems. However, the quantitative estimates showing their real performance were lacking. The present paper concerns the first numerical investigation of methods which use these approximations. It is based on large-scale calculations and comparisons of the performance of low-order schemes with emphasis on steady-state high Reynolds number solutions of the Navier–Stokes equations. The study is aimed at estimating the accuracy and quality of the resulting numerical solutions, as well as the corresponding computational costs. Another goal is the examination of the CUD behavior in combination with different "non-CUD" elements (viscous terms discretizations, meshes, iteration or time stepping methods, algebraic solvers).

In Sections 2 and 3, the theoretical background of CUD-II-3, CUD-II-5, and the resulting schemes are briefly outlined for completeness (the relevant mathematics can be found in [8–10]).

Testing calculations using the inviscid and viscous Burgers equation are described in Section 4. Their aims are estimates of the CUD "peak" performance which illustrate the main theoretical features of the technique (conservation, accuracy, behavior in the cases of discontinuous and steep gradient solutions), as well as comparisons with the second-order upwind scheme obtained by replacing the CUD with three-point one-sided differences. Although the emphasis is placed here on the mesh-convergence of steady-state viscous solutions, an example of inviscid shock-capturing calculations is also presented.

In Section 5, a family of implicit unfactored CUD-based schemes is outlined for the compressible Navier–Stokes equations written in curvilinear coordinates. In those schemes, the CUD approximations are used in the flux-splitting manner while the implicit operator is based on the first-order upwind differencing. For infinite values of time steps, the schemes reduce to defect-correction methods which are strictly contractive at least in 1D constant coefficient case.

Section 6 contains a detailed description of the calculations and the results. As a representative example, transonic cascade flow was chosen. Numerical experiments were carried out with refining meshes until the mesh-converged flow field was obtained. Using this field as a reference, the mesh-convergence rates, actual accuracy, and computational costs of the CUD-II-3, CUD-II-5, and the second-order scheme are estimated and compared. The flow field parameters are presented for different meshes, special attention being paid to the separate flow resolution near the trailing edge.

Finally, Section 7 summarizes the main findings of the paper and presents the discussion.

2. NONCENTERED THIRD- AND FIFTH-ORDER COMPACT UPWIND DIFFERENCING

Compact upwind differencing is thought of here as an implicit nonsymmetric discrete form of convective terms of fluid dynamics-type equations which satisfies two conditions:

(i) The implicit part consists of tridiagonal operators ("compactness").

(ii) The "orientation" of the differencing can be changed in the same way as in the case of conventional one-sided differences. From the mathematical viewpoint it means that the differencing operator can change the sign of its self-adjoint part from positive to negative or vise versa.

We will focus here on the latest versions of the CUD family [8, 9] which are investigated in the present study. They can be considered as additive corrections to the general first-order upwind differencing operators, defined on the mesh $x_j = jh$, $h = \text{const}$ as

$$\Delta(s) = 0.5(\Delta_0 - s\Delta_2), \tag{1}$$

where

$$\Delta_0 f_j = f_{j+1} - f_{j-1},$$
$$\Delta_2 f_j = f_{j+1} - 2f_j + f_{j-1},$$

and s is the "switching" parameter.

The corrected differencing formulas can be obtained in the following way.

Considering the difference between the exact derivative $D_x = \partial/\partial x$ and the generic operator $\Delta(s)$, we may write the formal Taylor expansion series regarding h as a small parameter:

$$D_x - h^{-1}\Delta(s) = \frac{sh}{2}D_x^2 - \frac{h^2}{6}D_x^3 + \frac{sh^3}{24}D_x^4 - \frac{h^4}{120}D_x^5 + O(h^5)$$
$$= \left(I - \frac{1}{3s}hD_x + \frac{1}{12}h^2D_x^2 - \frac{1}{60s}h^3D_x^3\right)\frac{sh}{2}D_x^2 + O(h^5). \tag{2}$$

Here we suppose that $s \neq 0$. The next step is to change the power series

$$1 - \frac{1}{3s}z + \frac{1}{12}z^2 - \frac{1}{60s}z^3 \tag{3}$$

by a suitable Padé approximant, $z = hD_x$ being considered as a variable.

If the third-order accuracy for the LHS of (2) is sufficient, then expression (3) can be changed by

$$\left(1 + \frac{1}{3s}z\right)^{-1}$$

which is $O(z^2)$ Padé approximant for (3). All we need now is to discretize hD_x and $h^2D_x^2$ at least with the first- and second-order formulas, respectively. Restricting our consideration to tridiagonal operators, we take Δ_2 and $\Delta(s_1)$ as the discretization of $h^2D_x^2$ and hD_x, respectively, considering s_1 as another parameter. Now we have the third-order operator

$$L_3 = \left[\Delta(s) + \frac{s}{2}\left(I + \frac{1}{3s}\Delta(s_1)\right)^{-1}\Delta_2\right]\Big/h. \tag{4}$$

Including more terms in the Padé approximants for the RHS of Eq. (2), the fifth-order CUD operator which will be used also in the present study can be written as

$$L_5 = \left[\Delta(s) + \frac{s}{2}R^{-1}Q\left(I + \frac{1}{12}\Delta_2\right)^{-1}\Delta_2\right]\Big/h, \tag{5}$$

where

$$Q = I + \left(-\frac{1}{15s} - \frac{s_1}{4}\right)\Delta_0 + \left(\frac{1}{6} + \frac{s_1}{15s}\right)\Delta_2$$

$$R = I + \left(\frac{1}{10s} - \frac{s_1}{4}\right)\Delta_0 + \left(\frac{1}{6} - \frac{s_1}{10s}\right)\Delta_2$$

$$\operatorname{sign} s_1 = \operatorname{sign} s, \quad s^2 = 4/5.$$

Supposing that u is a sufficiently smooth function and using the Taylor expansion series, the following expressions can be obtained when estimating the actions of the CUD-II-3 and CUD-II-5 operators,

$$L_3u_j = D_xu\Big|_{x=x_j} + s\left(\frac{1}{12}\frac{s_1}{s} + \frac{1}{18s^2}\right)h^3\frac{\partial^4u}{\partial x^4}\Big|_{x=x_*}, \tag{6}$$

$$L_5u_j = D_xu\Big|_{x=x_j} - s\left(\frac{1}{144}\frac{s_1}{s} + \frac{1}{900s^2}\right)h^5\frac{\partial^6u}{\partial x^6}\Big|_{x=x_*}, \tag{7}$$

where $x_* \in [x_j - h, x_j + h]$. One can observe that the numerical coefficients in (6), (7) with proper choice of s_1 and s can be considerably smaller then those in conventional formulas of the same orders. It means that approximations (6), (7) to D_xu can be quite accurate.

It can be proved also that L_m, $m = 3, 5$, is a positive (negative) operator if $s > 0$ ($s < 0$) and sgn $s_1 =$ sgn s[10]. In that case, $(L_m u, u)_H > 0$ for $s > 0$, $(L_m u, u)_H < 0$ for $s < 0$, where $u \neq 0$ and $(u, v)_H$ is the inner product defined as

$$(u, v)_H = \sum_i u_i v_i, \quad u, v \in H. \tag{8}$$

In (8), H is supposed to be the Hilbert space of either periodic or finitely supported scalar or vector-valued grid functions and the summation is performed over the grid points.

Denoting the skew-symmetric and self-adjoint parts of L_m by $L_m^{(1)}$ and $L_m^{(0)}$, it is easy to show that

$$L_m(s) = L_m^{(1)} + sL_m^{(0)}, \tag{9}$$

where $L^{(1)} = -(L^{(1)})^*$, $L^{(0)} = (L^{(0)})^* > 0$, and the asterisk denotes conjugate operators in the sense of the inner product $(.,.)_H$ defined by (8).

Note that the generic operator $\Delta(s)$ possesses the same property since $\Delta_0^* = -\Delta_0$ and $\Delta_2^* = \Delta_2 < 0$. That is why each L_m operator can be labelled by "upwind" differencing, meaning that its sign can be chosen according to the local slopes of characteristics of hyperbolic equations or systems. Looking at (9) from another side, one can say that L_m is the centered $(m + 1)$th order differencing defined by $L_m^{(1)}$ plus the mth-order dissipation defined by $L_m^{(0)}$. It is the main difference between L_m and the corresponding well-known centered compact differencing of the $(m+1)$th order which is dissipation-free (a rich variety of centered compact operators is presented in [13]).

Considering s as an upwinding parameter, we will refer to operators (4) and (5) as compact upwind differencing of the second type, (CUD-II-3) and (CUD-II-5), to discern them from the previous versions of third- and fifth-order CUD described in [10].

To outline other properties of operators L_3 and L_5, we consider the scalar conservation law

$$\frac{\partial u}{\partial t} + \frac{\partial f(u)}{\partial x} = 0 \tag{10}$$

and semi-discretized CUD scheme

$$\frac{\partial u}{\partial t} + L_m f(u) = 0, \tag{11}$$

where sgn $s =$ sgn $f'(u)$ at each grid point. Assuming frozen coefficients, scheme (11) is stable in the L_2-norm (more precisely, in the discrete analogue of L_2-norm) generated by $(.,.)_H$ due to the positivity of L_m. For proper discretizations of $\partial u/\partial t$ in Eq. (11), scheme (11) will be either conditionally or unconditionally stable.

In the case of the vector conservation law (10), positive approximations to $\partial f/\partial x$ and stable scheme (11) can be constructed either by diagonalization of the Jacobian matrix $f'(u)$ or by flux splitting (see [10] for details). The latter approach is used in the present study.

Supposing that $f(u) = au$, $a =$ const > 0, one can estimate dispersion and dissipation properties of (11). Comparing the exact wave solution of (10)

$$u(x, t) = e^{-ik(x-at)}$$

with the corresponding exact solution of (11)

$$u(x_j, t) = e^{-dt} e^{ik(jh - a_* t)},$$

where a_* is the numerical phase velocity while $d = d(k)$ characterizes dissipation, one can obtain the functions a_*/a and $\bar{d}(\alpha) = dh/|a|$, $\alpha = kh$.

Considering α as the Fourier variable and introducing the Fourier images $\hat{L}_m^{(1)}$ and $\hat{L}_m^{(0)}$ of $L_m^{(1)}$ and $L_m^{(1)}$ (which are imaginary and positive real functions of α, respectively), one can see that

$$a/a_* = \mathrm{Im}(\hat{L}^{(1)}(\alpha))/\alpha, \quad \bar{d} = |s|\hat{L}^{(0)}(\alpha).$$

The functions a/a_* and $\bar{d}$ are presented in [10] for various members of CUD family. Here we note only the following features of CUD-II-3 and CUD-II-5:

(i) In the domain of physically relevant wave numbers supported by meshes (approximately, for $0 \le \alpha \le \pi/2$), one has

$$a/a_* \approx 1, \quad \bar{d} \approx 0,$$

at least for fifth-order schemes which means negligible phase errors and dissipation;

(ii) For the shortest waves admitted by meshes ($\pi/2 \le \alpha < \pi$), the phase errors become apparent, but at the same time the dissipation increases dramatically. In fact, $L_m^{(0)}$ define mth-order built-in filter of high frequency noise.

3. DIFFERENCE SCHEMES

Considering again the scalar conservation law, we note that if the upwinding parameter s does not change its sign then the grid function $L_m f$ can be cast in the flux form

$$L_m f_j = q_{j+1/2} - q_{j-1/2}, \quad m = 3, 5$$

with the grid function $q_{j-1/2}$ ($j = 0, \pm 1, \pm 2, \ldots$), implicitly depending on f_j. To preserve this property in the case of sonic points, it is possible either to modify the generic operator $\Delta(s)$ [10], or to use the splitting technique. We will focus here on the latter approach, setting

$$\frac{\partial f}{\partial x} = L_m^+ \frac{f(u) + Cu}{2} + L_m^- \frac{f(u) - Cu}{2} + O(h^m), \quad m = 3, 5, \tag{12}$$

where the operators L_m^+ and L_m^- correspond to L_m with $s > 0$ and $s < 0$, respectively, C is some positive constant, and the index j is omitted.

To guarantee the positivity of this differencing operator, $f'(u) + C$ and $f'(u) - C$ do not need to be necessary positive and negative, respectively. Indeed, it is easy to verify that approximation (12) to $\partial f/\partial x$ is positive (in the "frozen coefficients" sense) for arbitrary $C > 0$.

Combining this approximation with any reasonable time-stepping device one can obtain a rich variety of CUD-II-m schemes for Eq. (10). For example, the simplest explicit

scheme reads

$$\frac{u^{k+1}-u^k}{\tau}+L_{mx}f^k=0, \tag{13}$$

where the mesh $\{t_k=k\tau, x_j=jh\}$ is supposed; $L_{mx}f$ stands for the approximation to $\partial f/\partial x$ given by (12). To obtain u^{k+1}, two and four tridiagonal matrices should be inverted when computing the actions of the operators L_{3x} and L_{5x}, respectively. To do so, some numerical boundary conditions are needed at the boundary points. They can be obtained in several ways by using, for example, one-sided compact or conventional differencing formulas. However, care should be taken to preserve the stability of the schemes.

Another example is the Runge–Kutta explicit procedure which was used in the unsteady calculations for the inviscid Burgers equation described below.

In the present paper we, however, will focus on the implicit scheme

$$[I+\tau L_1 f'(u^k)]\frac{u^{k+1}-u^k}{\tau}+L_{mx}f^k=0. \tag{14}$$

In Eq. (14), L_1 is the first-order operator which can be obtained from Eq. (12) by using $\Delta(|s|)$ and $\Delta(-|s|)$, instead of L_m^+ and L_m^-, respectively. The truncation error of scheme (14) is $O(\tau+h^m)$ which is suitable for steady-state computations with the possible detection of unsteady behavior of solutions.

The tridiagonal operator $I+\tau L_1 f'(u^k)$ should be inverted to obtain u^{k+1}, once the action $L_{mx}f^k$ is calculated.

It was proved in [9] that scheme (14) is unconditionally stable in the case of "frozen" coefficients ($f'(u^k)=a=\text{const}$). Moreover, the operator $G: u^k \to u^{k+1}$ obtained from (14) when $\tau=\infty$ is strictly contractive; that is, $\|G\|\le K<1$. It was shown [10] that $K(s,s_1)=3/(3+2s_1/s)$ in the case of CUD-II-3, which means rapid convergence of the iterative process (14) with L_3. It is the main advantage of the L_3 operator over L_5 and other CUD operators. For the best choices of the upwinding parameters, their contractivity numbers $K<1$ are very close to unity [10].

Schemes (13), (14) can be easily extended to the cases of the vector conservation laws with viscous terms. Supposing that u and f in Eq. (10) are p-vectors, the positivity of the discretization of $\partial f/\partial x$ will be guaranteed if the constant C is changed by any constant symmetric matrix with positive eigenvalues. Moreover, the term Cu can be changed by some vector-valued function $\mathbf{B}(\mathbf{u})$ for which the Jacobian matrix $\mathbf{B}'(\mathbf{u})>0$ has positive eigenvalues. In particular, the well-known forms of the flux splitting are possible when doing so. We emphasize, however, that from the stability viewpoint there is no need for the positivity and the negativity of the $\mathbf{f}'(\mathbf{u})+\mathbf{B}'(\mathbf{u})$ and $\mathbf{f}'(\mathbf{u})-\mathbf{B}'(\mathbf{u})$ eigenvalues, respectively.

Supposing, further, that viscous terms are included in Eq. (10), one can discretize these terms in many ways quite independently of $\partial f/\partial x$. For example, the term $\partial/\partial x(\mu\partial u/\partial x)$ can be discretized as

$$\frac{\partial}{\partial x}\mu\frac{\partial u}{\partial x}\approx -\delta_x\mu\delta_x^* u, \tag{15}$$

where δ_x and δ_x^* are some differencing operators and their adjoint operators, respectively. Setting $\delta_x=A(s)^{-1}\Delta(s)$, $\delta_x^*=-A(-s)^{-1}\Delta(-s)$, where $A(s)$ is the tridiagonal CUD-3 operator [10], one obtains third-order approximation to (15) based on CUD-3. It was used

previously as a part of the CUD-3 scheme for compressible Navier–Stokes equations [2]. It was found, however, that in many cases conventional second-order discretization does not notably decrease the accuracy of the CUD-3 scheme as far as high Reynolds number flows are concerned and the proper condensing of grid points in viscous layers is performed.

We note, finally, that to construct the CUD schemes in the case of several spatial coordinates (say x, y, and z), it is sufficient to use CUD operators corresponding to each space directions (L_x, L_y, and L_z, respectively). By doing so, one can guarantee the positivity of spatial discretizations (in the "frozen coefficients" sense). Multidimensional upwinding is also possible but this topic is beyond the scope of the present paper.

4. NUMERICAL EXPERIMENTS WITH BURGERS EQUATION

To investigate the property of CUD-II-3 and CUD-II-5 approximations numerically, we consider first the Burgers equation,

$$\frac{\partial u}{\partial t} + \frac{\partial}{\partial x}\left(\frac{u^2}{2}\right) = \nu \frac{\partial^2 u}{\partial x^2} + g(u, x), \tag{16}$$

where $g(u, x)$ is a forcing term.

Setting $\nu = 0$, one can verify the conservation of the above-described differencing when computing unsteady discontinuous solutions.

Unsteady inviscid case. Although CUD approximations were designed primarily as methods for the Navier–Stokes equations, CUD calculations for inviscid cases are useful illustrations of their properties. The shock-capturing capabilities of some CUD-3 schemes were studied in [5, 6]. The results for fifth-order CUD are presented in [10]. Avoiding the reproduction of these data here, we summarize the main conclusions:

(i) In accordance with the Godunov's theorem, CUD-based schemes are not monotone in the unsteady inviscid case. However, due to their upwind nature, spurious oscillations are well-localized near shocks.

(ii) Application of flux limiters removes the wiggles completely, limiters being activated only near shocks.

The above observation suggests the possibility of using CUD as a part of high resolution schemes.

In this paper, we present an example allowing us to compare quantitatively the numerical solutions obtained in [14] and the CUD-II-5 results. The problem is given by Eq. (16) with $\nu = 0$, $g(u, x, t) = 0$,

$$u(x, 0) = 1 + 0.5 \sin(\pi x), \quad x \in [-1, 1],$$

and periodic boundary conditions. For this problem, the tabulated errors for several values of t and mesh sizes are presented in [14].

Table 1 shows the estimates of accuracy in L_1 (obtained by comparing with the exact solution) extracted from [14] and calculated using CUD-II-5 with the fourth-order Runge–Kutta method. The values listed in the Table 1 correspond to $t = 0.3$ when the exact solution is smooth. They are obtained for the numbers of grid points $n = 80$, 160, 320, 640, and 1280. No limiters were used in the CUD case.

TABLE 1

n	L_1 err, [14]	L_1 order, [14]	L_1 err, CUD-II-5	L_1 order, CUD-II-5
80			7.0102D-07	
160	4.6548D-06		3.6185D-08	4.27
320	7.7529D-07	2.59	2.0451D-09	4.14
640	1.2524D-07	2.63	1.2145D-10	4.08
1280	1.8075D-08	2.83	7.6772D-12	3.98

As can be seen from the Table 1, the CUD results are up to two to three orders of magnitude more accurate than those obtained using the third-order TVB scheme [14] with the same mesh sizes.

The estimated mesh-convergence orders in our case vary from 3.98 to 4.27, thus, indicating rather fast convergence. A fifth-order convergence is not seen here due to the dominance of $O(\tau^4)$ errors of the Runge–Kutta method over $O(h^5)$ errors of the CUD.

Figure 1 shows the CUD-II-5 and the exact solutions at $t = 1.1$ when the shock is already formed. In these calculations, flux limiter [15] was used to remove several wiggles near the shock.

It should be noted that the behavior of solutions near discontinuities depends strongly on the type and parameters of the limiters used in calculations. No attempt has been made in the present study to optimize the monotonization process.

Steady-state solutions of modified Burgers equation. In the steady-state case, Godunov's theorem is no longer applicable and nonmonotone schemes can provide wiggle-free

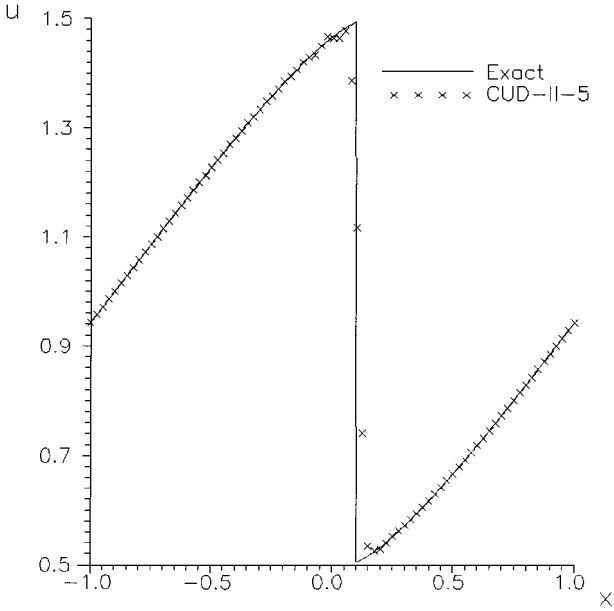

FIG. 1. Solution of the inviscid Burgers equation at $T = 1.1$ CUD-II-5 with the fifth-order Runge–Kutta time stepping.

discontinuous solutions. Indeed, examples may be easily produced, showing that standing shock grid functions without any oscillations can be exact solutions of difference equations.

In the viscous case, the monotonicity properties of the steady-state numerical solutions of (16) depend on the cell Reynolds number $\mathrm{Re_c} = u_* h/\nu$, where u_* is some reference value of u. To estimate the influence of $\mathrm{Re_c}$, it is worth performing the simplest linear analysis.

Consider the equation

$$\frac{\partial u}{\partial t} + a\frac{\partial u}{\partial x} = \nu\frac{\partial^2 u}{\partial x^2} \tag{17}$$

with $\partial u/\partial t = 0$, $a = \mathrm{const}$, and $u(0) = 1$, $u(1) = 0$. The exact solutions of algebraic systems resulting from any discretization are known to have the general form $u_j = \sum_k c_k q_k^j$, where q_k is the kth root of the characteristic polynomial. Supposing that the spurious components $c_k q_k^j$, $k > 2$, are removed by a suitable choice of some additional boundary conditions for u_j and taking into account the boundary conditions in (17), one can easily obtain

$$u_j = \frac{q^N}{q^N - 1} - \frac{1}{q^N - 1} q^j, \quad j = 1, 2, \ldots, N, \tag{18}$$

where $q = q(\mathrm{Re_c})$ and $\mathrm{Re_c} = ah/\nu$.

All difference schemes possess the following property: if $\mathrm{Re_c} < \mathrm{Re_{c*}}$, where $\mathrm{Re_{c*}} = O(1)$ is some critical value then (18) mimics the exact solution of problem (17) given by

$$u(x) = \frac{\exp(a/\nu)}{\exp(a/\nu) - 1} - \frac{1}{\exp(a/\nu) - 1}\exp(ax/\nu).$$

If $\mathrm{Re_c} \to \infty$ then the behavior of numerical solutions for different schemes can be completely different depending on the values of $q(\mathrm{Re_c})$. In the case of centered schemes one usually has $|q| \to 1$ when $\mathrm{Re_c} \to \infty$. It means that solution (18) can be completely erroneous due to ill-conditioned nature of difference equations. If, however, $|q|$ is sufficiently large for $\mathrm{Re_{c*}} \le \mathrm{Re} \le \infty$, one may hope that at least the "inviscid" part of the solution is reproduced with reasonable accuracy due to rapid decay of possible wiggles. For example, in the case of CUD-II-3 and $s = s_1 = 1$ one has

$$q = \frac{\frac{4}{6} + \frac{5}{6}\mathrm{Re_c} + \left[\left(\frac{4}{3} + \frac{5}{6}\mathrm{Re_c}\right)^2 + \frac{2}{3}\mathrm{Re_c}\left(\mathrm{Re_c} - \frac{8}{3}\right)\right]^{1/2}}{\frac{8}{3} - \mathrm{Re_c}}.$$

If $\mathrm{Re_c} < \frac{8}{3} = \mathrm{Re_{c*}}$ then q is positive and u_j is oscillation-free. If $\mathrm{Re_c} > \frac{8}{3}$ then q is negative, $|q|$ being large tending to 2 when $\mathrm{Re_c} \to \infty$. Hence, the oscillations generated by the second term in the RHS of (18) have only marginal nature, decaying with increasing j.

The comparison of the steady-state results obtained when using conventional second-order and several CUD options are reported in [10, 16] for $g(u, x) = 0$. They show that the CUD-based methods can be up to several orders of magnitude more accurate than conventional ones. However, in these calculations, the inviscid and viscous terms are balanced mainly in the shock transition regions, the "inviscid" portion of the solution being nearly constant.

To add some complexity to the solution outside the shock, we consider the Burgers equation with a source term for which the exact solution is available.

The problem is formulated as

$$\frac{\partial u}{\partial t} + \frac{\partial}{\partial x}\frac{u^2}{2} = \nu\frac{\partial^2 u}{\partial x^2} - e^x\left[\frac{v}{2\nu}(v^2-1)(1-e^x) + v^2(1-e^x) + \nu v - 1\right]$$
$$v(x) = \tanh\left(\frac{1-2x}{4\nu}\right) \tag{19}$$
$$u(0,t) = \tanh\left(\frac{1}{4\nu}\right), \quad u(1,t) = -e\tanh\left(\frac{1}{4\nu}\right).$$

The exact steady-state solution of (19) is

$$u_e(x) = e^x v(x).$$

If the viscosity coefficient ν is small, two "inviscid" parts of the solution with the exponential behavior are separated by the shock transition region centered at $x = 0.5$, its width being $O(\nu)$. Since the "jump" of the solution δu and the maximum value of the derivative $u'(x)$ are approximately 3 and $1/2\nu$, respectively, we define the characteristic scale of the shock as $\delta u/u'(x) \approx 6\nu$. Hence, the number of grid points N_ν inside the shock in the case of uniform grids can be estimated as $N_\nu = 6\nu N = 6\nu/h$ when N is the total number of grid points. The parameter N_ν is, in fact, inversely proportional to the characteristic cell Reynolds number $\mathrm{Re_c}$ defined here by $u_* h/\nu$, where $u_* = 1$. The values of N_ν are given now by $N_\nu = 6/\mathrm{Re_c}$. Either N_ν or $\mathrm{Re_c}$ are useful parameters when presenting the numerical solutions, since, on the one hand, they indicate subcritical ($\mathrm{Re_c} < \mathrm{Re_{c*}}$) or supercritical ($\mathrm{Re_c} > \mathrm{Re_{c*}}$) regimes, followed from the linear analysis similar to that presented in Section 2 and, on the other hand, they show directly the mesh size h for $\nu = \mathrm{const}$.

Calculations were carried out using uniform meshes with double the number of grid points. The implicit time stepping defined by Eq. (14) was used. The processes were terminated when L_2-norms of the residuals became as small as 10^{-12}. The admissible CFL numbers were found to be up to 1000, thus indicating that the scheme is practically unconditionally stable in the present nonlinear case.

Along with the CUD-II-3 and CUD-II-5 approximations to the inviscid term, the second-order one-sided three-point formulas were tried, thus presenting the conventional upwind scheme. We denote it by UD-2. Two options were used when discretizing the viscous term, namely, the conventional second-order approximation of the type (15) and the fourth-order compact approximation

$$\nu\frac{\partial^2 u}{\partial x^2} = \frac{\nu}{h^2}\left(I + \frac{\Delta_2}{12}\right)^{-1}\Delta_2 u + O(h^4). \tag{20}$$

In the case of UD-2, the above options gave approximately the same results so the "pure" second-order upwind scheme was adopted as UD-2.

The main output of the calculations presented here are the numerical solution errors as functions of N_ν, where the error E_2 is defined on the basis of the deviations from the exact solution u_e of Eq. (19):

$$E_2 = \left[h\sum_{i=1}^{N}(u_i - u_e(x_i))^2\right]^{1/2}.$$

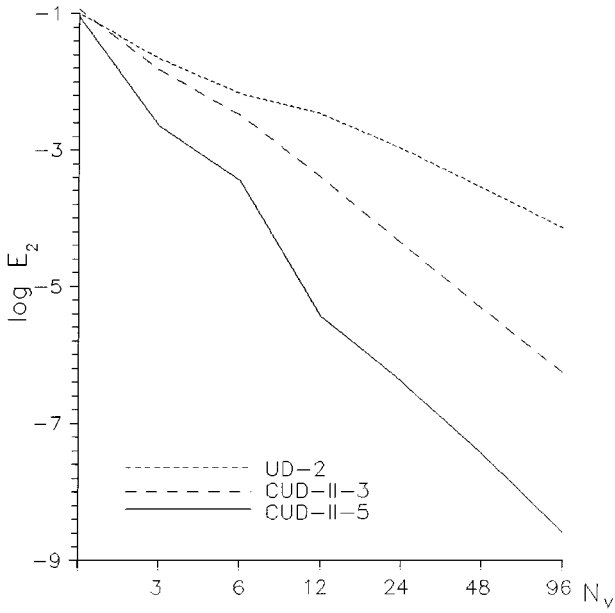

FIG. 2. L_2-errors of the steady-state solutions of the modified Burgers equation vs the number of grid in the shock region: comparisons of CUD-II-5, CUD-II-3, and UD-2 convergence curves.

Figure 2 shows the log–log plot of $E_2(N_v)$ for CUD-II-5, CUD-II-3 with fourth-order discretization (20), and UD-2. Depending on the values of N_v, the numerical solutions of Fig. 2 can be classified into those which resolve or underresolve the shock. Taking into account the above linear analysis, we define the underresolved case by the inequality $\mathrm{Re}_c \geq \mathrm{Re}_{c*} = 2$ which gives $N_v \leq 3$.

As can be seen from the figure, the E_2-errors for the CUD-based schemes are not only decaying more rapidly than those for UD-2 in the well-resolved region(which is quite expected), but they also show the dramatic increase of accuracy measured by the orders of magnitude. Comparing the CUD-II-5 and CUD-II-3 solutions, one can see that the third-order results are less accurate but they are considerably more accurate than those obtained with UD-2.

Considering now the underresolved case when only one to three points can be found in the shock transition region, all considered methods give approximately the same values for the E_2-errors. However, the CUD-II-5 error is slightly less than that for other tested methods. It is not a trivial fact, since large high-order derivatives in truncation errors can completely neutralize the powers of mesh sizes in the case of coarse meshes.

A close examination of the underresolved case when only one grid point can be found strictly inside the shock ($N = 25$, $\mathrm{Re}_c = 4$) has shown that all methods give the solutions which slightly oscillate near the exact solution $u_e(x)$. This fact fits neatly into the above theoretical estimates. However, the E_2 errors in this case are not excessively large, thus indicating relatively small amplitudes of these spurious oscillations.

To restore the noticeable advantage of CUD-based schemes, it is sufficient to condense grid points in the shock region. Figure 3 shows the comparison of the exact solution (solid line) and CUD-II-5 (markers) in the case of $N = 10$ and clustering which guarantees about three grid points in the shock.

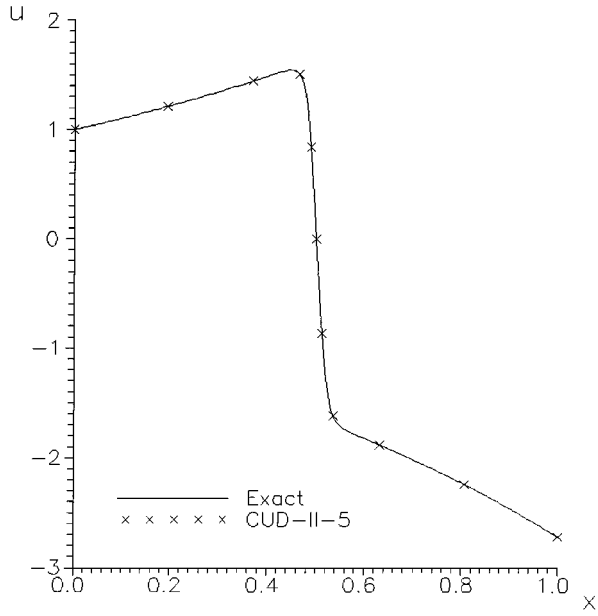

FIG. 3. The exact and CUD-II-5 steady-state solutions of the modified Burgers equation. $N = 10$, with clustering of grid points in the shock region.

Returning to the well-resolved case, one can see that the slopes of the CUD curves are not strictly constant, showing a slight variation of the convergence rates. It can be explained by the "blended" nature of the truncation errors (TE) which have the form

$$TE(x) = TE^m_{\text{inv}} + \nu TE^n_{\text{vis}}, \quad TE^m_{\text{inv}} = c_1(x)h^m, \quad TE^n_{\text{vis}} = c_2(x)h^n,$$

where $m = 3, 5$ and $n = 4$ while the functions $c_i(x)$, $i = 1, 2$, are defined by the exact solution. In contrast to the inviscid and viscous terms of the equation, TE^m_{inv} and TE^n_{vis} do not balance each other and their relative roles depend strongly on the c_1 and c_2 functions. As a result, one may expect mth- or nth-order convergence if $TE_{\text{inv}} >> \nu TE_{\text{vis}}$ or $TE_{\text{inv}} << \nu TE_{\text{vis}}$, respectively.

To investigate further the role of the viscous term discretization, additional calculations were carried out using the conventional second-order three-point approximation to $\partial^2 u/\partial x^2$ and the sixth-order compact differencing,

$$\frac{2}{15}u''_{j-1} + \frac{11}{15}u''_j + \frac{2}{15}u''_{j+1} = \frac{1}{h^2}\left[\frac{1}{20}u_{j-2} + \frac{4}{5}u_{j-1} - \frac{17}{10}u_j + \frac{4}{5}u_{j+1} + \frac{1}{20}u_{j+2}\right] + O(h^6),$$

where the primes denote derivatives. The convergence curves of CUD-II-5 with the $O(h^n)$ formulas for the viscous term, $n = 2, 4, 6$, are shown in Fig. 4 with the UD-2 results from Fig. 2.

The following conclusions may be drawn from Figs. 2 and 4:

(i) the CUD-based schemes are considerably more accurate than UD-2, even though a low-order operator is used for the viscous term;

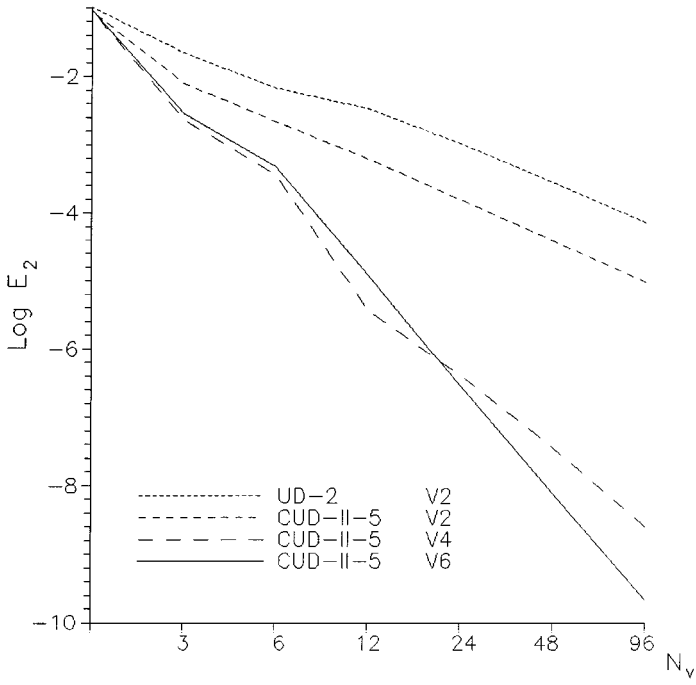

FIG. 4. Comparisons of mesh convergence for different discretization of the viscous terms CUD-II-5 with second- (V2), fourth- (V4), and sixth-order (V6) discretization of viscous terms.

(ii) the combination $m = 5, n = 6$ provides the most rapid convergence and the least errors for large N_v. However, the CUD-II-5 curves corresponding to $n = 4$ and $n = 6$ have intersections in some domain of N_v due to the combined effect of the "viscous" and "inviscid" truncation errors.

Again, the explanation follows from the relative roles of TE^m_{inv} and TE^n_{vis}. Table 2 shows the numerical values of their L_2 norms calculated using the exact solution for $N = 1600$.

Due to $TE^5_{\text{inv}} << \nu TE^4_{\text{vis}}$, $TE^5_{\text{inv}} >> \nu TE^6_{\text{vis}}$, and $TE^3_{\text{inv}} >> \nu TE^4_{\text{vis}}$, the convergence near $O(h^5)$, $O(h^4)$, or $O(h^3)$ can be expected for the different combinations of m and n.

Since νTE^2_{vis} dominates over TE^m_{inv}, $m = 3, 5$, both CUD schemes are expected to be of second order as in the case of UD-2. However, $TE^2_{\text{inv}} >> \nu TE^2_{\text{vis}}$ and large "inviscid" errors make the actual accuracy of UD-2 considerably poorer (about an order of magnitude) than the accuracy of its CUD counterparts.

The estimates of the L_2 convergence orders calculated for different combinations of m and n (denoted by $m - n$) and large N_v are presented in Table 3.

As can be seen, the actual order of the $m - n$ combination lays between m and n or near n.

TABLE 2

TE^5_{inv}	TE^3_{inv}	TE^2_{inv}	νTE^6_{vis}	νTE^4_{vis}	TE^2_{vis}
9.05D-08	1.2D-04	1.25D-02	1.46D-09	1.05D-06	1.95D-03

TABLE 3

$m-n$	$5-6$	$5-4$	$5-2$	$3-4$	$2-2$
L_2-order	5.15	3.84	2.47	3.11	1.96

Based on the above observations, one may arrive at the conclusion that the CUD technique can be advantageous even when combined with simple viscous term discretizations in the cases of high Reynolds number flows. In these cases, the dominance of $O(h^m)$, $m = 3, 5$, truncation errors in inviscid portions of the flow due to the Re^{-1} factor and the absence of the dominant errors of the convective term discretizations in viscous regions may increase solution accuracy. This suggestion will be illustrated in the next section.

We conclude this section with the following remarks:

1. The exact solution Eq. (19) is characterized by a rather strong shock inside the inviscid flow. To estimate roughly the accuracy in the "smooth" cases, one can consider $N_v = 6/\mathrm{Re_c}$ as a number of grid points per characteristic length. For example, if there is no shock in the computational domain $0 \le x \le 1$ then $N_v = N$ and the efficient $\mathrm{Re_c} = 6/N$.

2. The local errors in the shock region influence greatly the E_2 error. Clearly, the local errors in the "inviscid" parts of the solutions are considerably less than E_2 for fixed values of $\mathrm{Re_c}$.

5. APPLICATION TO COMPRESSIBLE NAVIER–STOKES EQUATIONS

We consider the Navier–Stokes equations written in conservative form in general curvilinear coordinates ξ, η, ζ as

$$\frac{\partial \mathbf{f}(\mathbf{u})}{\partial t} + \frac{\partial \mathbf{E}(\mathbf{u})}{\partial \xi} + \frac{\partial \mathbf{F}(\mathbf{u})}{\partial \eta} + \frac{\partial \mathbf{G}(\mathbf{u})}{\partial \zeta} = \mathbf{V}(\mathbf{u}), \tag{21}$$

where $\mathbf{u} = (\rho, u, v, w, \epsilon)^T$ with Cartesian components of the velocity u, v, w, density ρ, and internal energy ϵ. The vectors $\mathbf{E}$, $\mathbf{F}$, $\mathbf{G}$, and $\mathbf{V}$ representing the flux functions and viscous terms, respectively, can be found in the CFD literature.

Introducing uniform mesh $\xi_i = i\,\Delta\xi$, $\eta_j = j\,\Delta\eta$, and $\zeta_k = k\,\Delta\zeta$, the CUD-II-m differencing described in Section 2 can be applied to ξ-, η-, and ζ-derivatives, resulting in the grid functions $L_{m\xi}\mathbf{E}$, $L_{m\eta}\mathbf{F}$, and $L_{m\zeta}\mathbf{G}$. Considering, for example, the ξ-direction, one can write

$$\frac{\partial \mathbf{E}(\mathbf{u})}{\partial \xi} \approx L^{+}_{m\xi}\left(\frac{\mathbf{E} + C\mathbf{f}(\mathbf{u})}{2}\right) + L^{-}_{m\xi}\left(\frac{\mathbf{E} - C\mathbf{f}(\mathbf{u})}{2}\right), \quad m = 3, 5, \tag{22}$$

where C is some positive symmetric matrix and $L^{\pm}_{m\xi}$ are the $L_{m\xi}$ operators corresponding to the parameters $\pm|s|$. The simplest choice of C is the diagonal matrix

$$C = c\lambda^{\xi}_{\max} I, \tag{23}$$

where $\lambda^{\xi}_{\max} = \max|\Lambda(\mathbf{E}'(\mathbf{u}))|$ and $\Lambda(\mathbf{E}'(\mathbf{u}))$ stand for the eigenvalues of $\mathbf{E}'(\mathbf{u})$. The constant c in Eq. (23) is of an order of unity and can be specified to a certain extent arbitrarily. Theoretically, the reasonable choices of C and c are not expected to influence noticeably

the numerical solutions in "smooth" regions, since the term $C\mathbf{f}(\mathbf{u})$ in Eq. (22) corresponds to the mth order dissipative mechanism acting only on short-wave harmonics. Of course, other forms of $C\mathbf{f}(\mathbf{u})$ (or $\mathbf{B}(\mathbf{u})$) are possible.

Considering viscous term discretizations, numerical examples presented in the previous section show the beneficial role of high-order techniques. Having in mind this strategy, we nevertheless choose as the first attempt more simple conventional second-order differencing of the type

$$\left(\frac{\partial}{\partial\xi}\mu\frac{\partial\Phi}{\partial\xi}\right)_{ijk} = [\mu_{i+1/2}(\Phi_{i+1}-\Phi_i)-\mu_{i-1/2}(\Phi_i-\Phi_{i-1})]_{jk}$$
$$\mu_{i\pm1/2} = (\mu_{i\pm1}+\mu_i)/2$$

for any grid function μ and Φ. In this way, it is possible to see how CUD operators perform with low-order approximations of viscous terms in the case of high Reynolds number flows.

Due to the conservative property of L_m^+ and L_m^-, the difference analogues of the spatial derivatives in (21) can be considered as the balance of fluxes across the faces of the computational cells centered at each (i, j, k) grid point. However, no special measures were undertaken to preserve the geometrical conservation laws. It was expected that violation of these laws in the case of high-order schemes would lead only to high-order influence on numerical results, at least in the case of smooth solutions. To verify this assumption, CUD-II-3 was applied to the chain rule conservation laws. It was found that no considerable difference between numerical solutions can be observed in the cases of transonic cascade flows when using highly skewed curvilinear coordinates.

In all cases, denoting the CUD discretization of the spatial derivatives in Eq. (21) by $N\mathbf{u}$, the semi-discretized form of Eq. (21) can be cast in the form

$$\frac{\partial\mathbf{u}}{\partial t} + M^{-1}N\mathbf{u} = 0, \tag{24}$$

where M is the Jacobian matrix $\mathbf{f}'(\mathbf{u})$. Starting from Eq. (24), the final scheme can be written as

$$(I+\tau\sigma N_1)\frac{\mathbf{u}^{k+1}-\mathbf{u}^k}{\tau} + M^{-1}N\mathbf{u}^k = 0, \tag{25}$$

where k denotes time level $t_k = k\tau$ with time step τ (in general, k and τ can be considered as iteration numbers and iteration parameters, respectively) while values $\sigma = 0$ and $\sigma = 1$ correspond to explicit and implicit schemes. In Eq. (25), N_1 is the first-order discretization of spatial derivatives of the linearized Navier–Stokes equations obtained when using the upwind operators $\Delta(s)$ defined in Section 2 and corresponding to ξ, η, and ζ coordinates. The stencil in the implicit operator $I+\tau\sigma N_1$ contains only three grid points in each spatial direction, thus admitting relatively simple iterative inversions.

We note that by setting $\tau = \infty$, $\sigma = 1$, scheme (25) can be transformed easily into a defect correction procedure with solving two or four nonlinear problems based on first-order operators to guarantee third- or fifth-order accurate results.

To invert the implicit operator in Eq. (25), any iterative solver for large sparse matrices can be used. The numerical experiments were carried out using GMRES method [17] with ILU preconditioner and Gauss–Zeidel technique. Of course, only a limited number

of iterations were performed during each time step (or external iteration), the iteration parameter τ being dependent on the grid points.

When constructing scheme (25), other operators (in particular, other members of the CUD family) can be used to descretize the spatial derivatives in Eq. (21). It makes comparisons of schemes based on different approximations being particularly simple.

6. NUMERICAL EXAMPLE: 2D FLOWS

To illustrate the performance of scheme (25) with the CUD approximations in the case of nonorthogonal curvilinear coordinates, the transonic cascade flow described by the Navier–Stokes equations was chosen as a target problem. This problem is interesting due to various types of boundary conditions, high curvature leading and trailing edges, and nonuniform skewed meshes. In the present study, the 2D case is considered only. It allows us to carry out large-scale calculations aimed at investigating the computational efficiency of the schemes and its dependence on various scheme parameters and details (grids, boundary conditions, etc.)

The computational domain typical of turbomachinery problems with periodic, solid wall, inflow, and outflow boundaries was considered. At the inflow, the total pressure, the total temperature, and the inflow angle were specified while the static pressure and the extrapolation conditions were used at the outflow. At the solid walls the no-slip condition and prescribed temperature were assumed.

The geometry of the blade and the H-type grid obtained by a parabolic grid generator is displayed in Fig. 5. To investigate the convergence of the steady-state solutions with refining meshes, 30×20, 59×39, and 117×77 grids were used. The time stepping procedure (more precisely, the external iterative procedure) was performed with the parameter τ in Eq. (25) considered as a variable grid function. The calculations were carried out for the transonic regime with the outlet static pressure to inlet total pressure ratio equal to 0.5. The Reynolds number Re varied from 10^4 to 1.6×10^6.

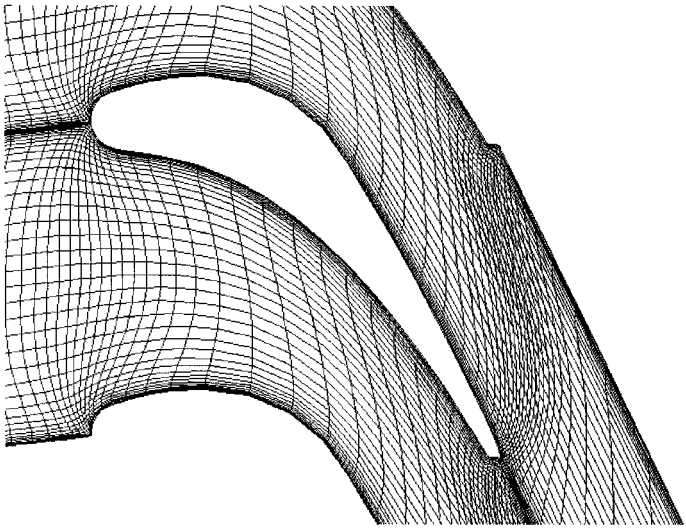

FIG. 5. H-type mesh used in cascade flow calculation.

Several boundary conditions for the wall pressure were tested, including the zero pressure gradient condition and the continuity equation at the wall. It was found that they provide practically the same flow fields everywhere but in the vicinity of the leading and trailing edges, where several percentage differences in the wall pressure distributions were observed. As a final option, the zero pressure gradient condition was adopted.

When advancing to the steady-state solutions, no attempts were made to optimize the time stepping processes. However, several options were tried, including the simplest explicit scheme ($\sigma = 0$) and implicit scheme ($\sigma = 1$) with the GMRES or Gauss–Zeidel iterations. It was found that, despite the fact that the GMRES option converges more rapidly, the Gauss–Zeidel technique is slightly preferable in the present particular exercises due to reduced operation counts per iteration.

As examples, several convergence histories are shown in Fig. 6, where L_2-norms of the residuals are presented as functions of the time step (the external iterations) number. It was found that very small residuals (up to 10^{-12}) can be obtained with great ease when using CUD-II-3. In accordance with the theoretical estimates [10], the slower convergence of the CUD-II-5 solutions may be seen from Fig. 6. For comparison, the curve for the explicit CUD-II-3 scheme (25) is also depicted in Fig. 6. It should be noted that, due to reasonable operation counts, all calculations of the present study were carried out on personal computers only.

Having in mind the advantages of the CUD-II-3 scheme when performing time-stepping and higher accuracy of CUD-II-5 steady-state solutions, the following approach may be suggested.

At the initial stage of computations, the CUD-II-3 block should be used to provide rapid convergence. This block should be replaced (by switching or gradually) with the CUD-II-5

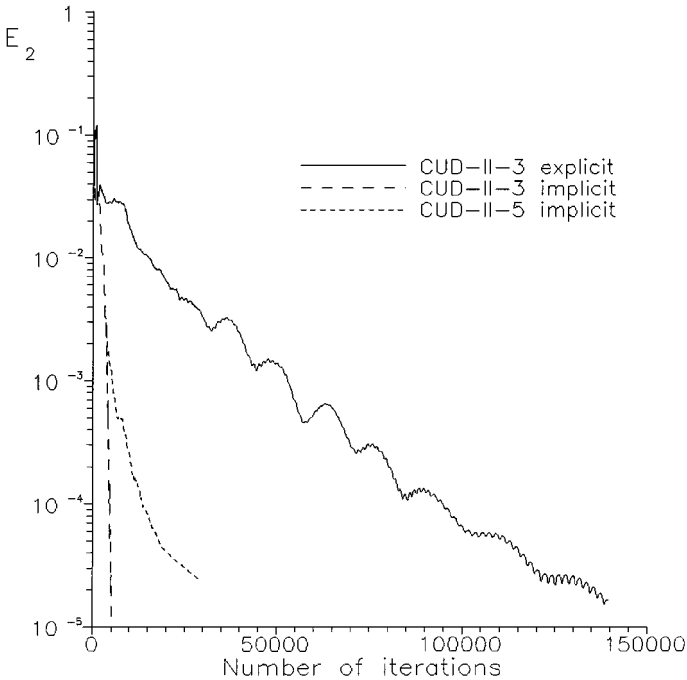

FIG. 6. Convergence to the steady-state solution: L_2 norms of the residuals vs the number of iterations.

one at the final stages of calculations, thus increasing the accuracy of steady-state solutions. Of course, many other elements may be added on the way to optimal algorithms, one of them being the multigrid strategy.

The main emphasis in the present study was placed on the convergence of stationary solutions obtained when applying the CUD technique to the hyperbolic part of the Navier–Stokes equations and preserving the conventional second-order discretization of the viscous terms. For comparison, the first- and second-order upwind differencing were also used in the framework of scheme (25). In both cases, L_m operators were changed, either by $\Delta(s)$ or by three-point one-sided formulas, to produce upwind schemes which we denote by UD-1 and UD-2, respectively.

The calculations were carried out starting with very coarse mesh 30×20 and then increasing the number of grid points by properly placing a new grid point between two old neighbor grid points. It was found that mesh 117×77 is sufficient to consider the CUD-II-5 solution as mesh-independent.

The general view of the flow field pattern is shown in Fig. 7, where the Mach number contours are presented.

The surface pressure distributions corresponding to the resolution 117×77 are shown in Fig. 8a for CUD-II-5, CUD-II-3, UD-2, and UD-1. As can be seen from the figure, the second-order results are sufficiently close to the mesh-converged curve while the first-order method performs badly.

The same distributions are shown in Figs. 8b and 8c for coarser meshes, 59×39 and 30×20. Note that the latter is too coarse to be used in standard cascade flow calculations. One may see that the CUD-II-5 curves for the 59×39 mesh only slightly deviated from the mesh-converged one. Surprisingly, the corresponding deviations in the case of the 30×20 mesh are also small enough to be well inside the typical scatter of experimental points for the cascade flows. This fact suggests very cheap Navier–Stokes calculations for engineering estimates.

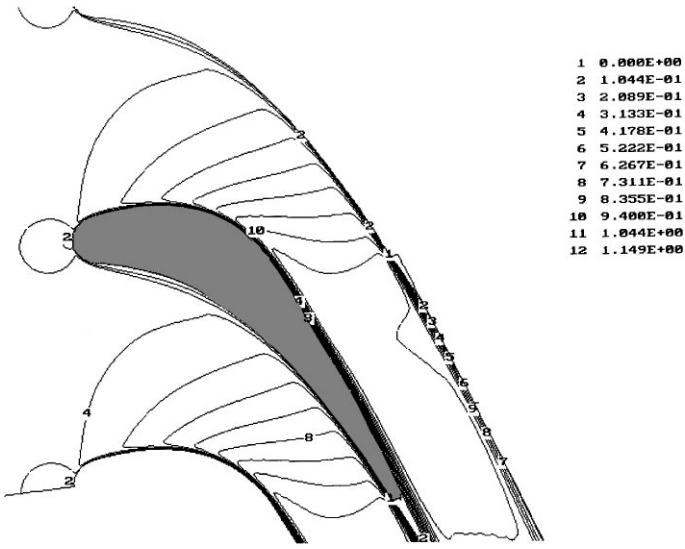

FIG. 7. Mach number contours.

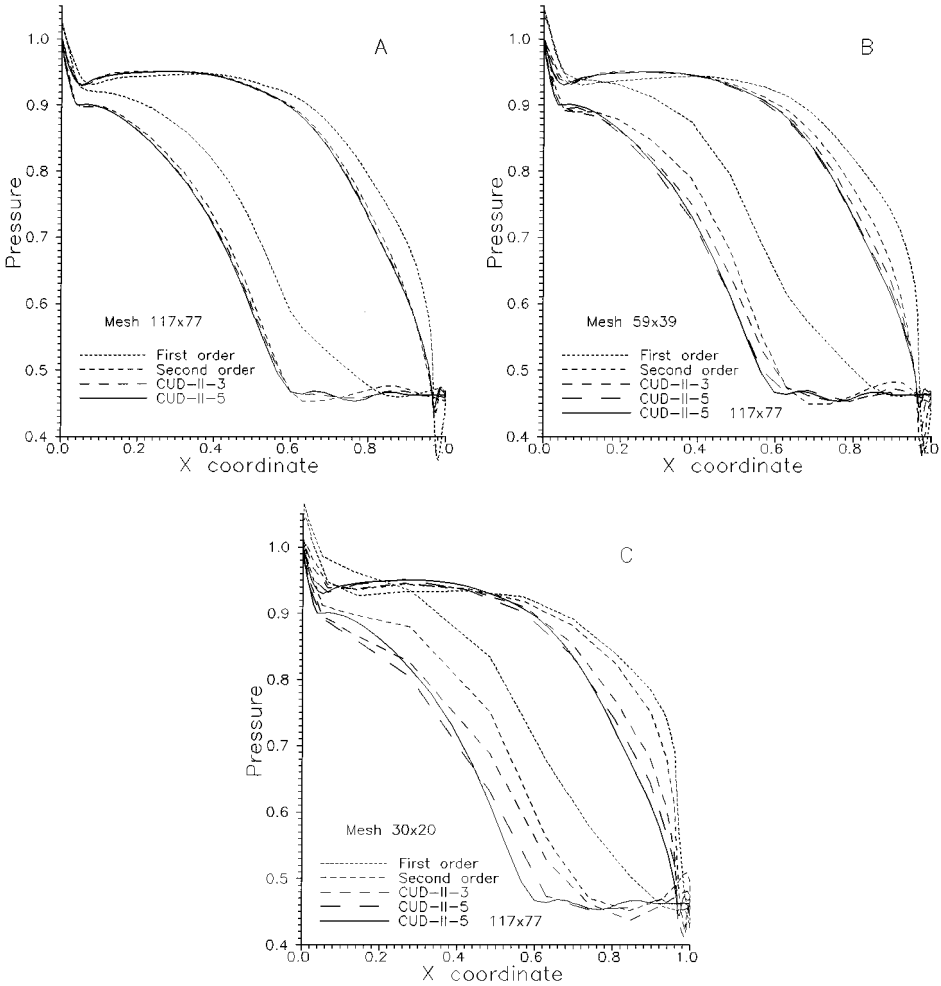

FIG. 8. Normalized surface pressure distributions. Meshes 117×77, 59×39, 30×20.

Considering UD-2 pressures, the differences between mesh-converged and coarser mesh data are quite pronounced (especially in the case of the resolution 30×20). The CUD-II-3 results are intermediate between those for CUD-II-5 and UD-2. However, mesh 59×39 seems to be quite acceptable for CUD-II-3 calculations.

The convergence of flow variables in the physical plane is illustrated in Figs. 9–11. As a representative characteristic, the Mach number distributions along the y-coordinates for $x = 0.3$ and $x = 0.9$ (the x-axis is collinear with the inflow direction, the origin being placed at the leading edge) are presented for CUD-II-3 and CUD-II-5 calculations. The markers show the grid points of the 30×20 mesh. Again, CUD-II-5 results exhibit good convergence, thus indicating that the coarsest mesh can be considered as acceptable for engineering estimates. Another observation is that no more than three to four grid points are needed in this case for accurate prediction of the tangential velocity near the surface.

As might be expected, the CUD-II-3 curves demonstrate slower convergence. Nevertheless, the 59×39 mesh seems to be quite reasonable for the scheme. For comparison, the

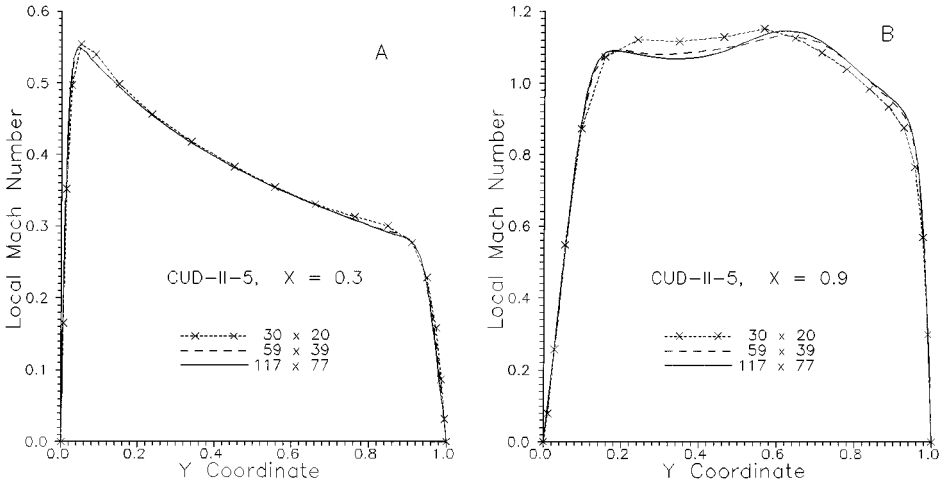

FIG. 9. Mach number distributions along $x = \text{const}$ for different meshes CUD-II-5.

UD-2 curve for a 30×20 mesh is also depicted in Fig. 11. It shows that the second-order scheme performs noticeably poorer than its CUD counterparts.

To estimate quantitatively the real orders of mesh convergence under the conditions of curvilinear coordinates and second-order discretizations of viscous terms, the deviations from the "exact" numerical solutions given by mesh-converged CUD-II-5 results were considered. They were defined as

$$\mathrm{err}_j = \frac{\left[\sum_i \left(\rho_i^{(j)} - \rho_i^{(3)}\right)^2 + \left(u_i^{(j)} - u_i^{(3)}\right)^2 + \left(v_i^{(j)} - v_i^{(3)}\right)^2 + \left(e_i^{(j)} - e_i^{(3)}\right)^2\right]^{1/2}}{\left[\sum_i \left(\rho_i^{(3)}\right)^2 + \left(u_i^{(3)}\right)^2 + \left(v_i^{(3)}\right)^2 + \left(e_i^{(3)}\right)^2\right]^{1/2}},$$

where the values of $j = 1, 2, 3$ correspond to meshes 30×20, 59×39, 117×77, and

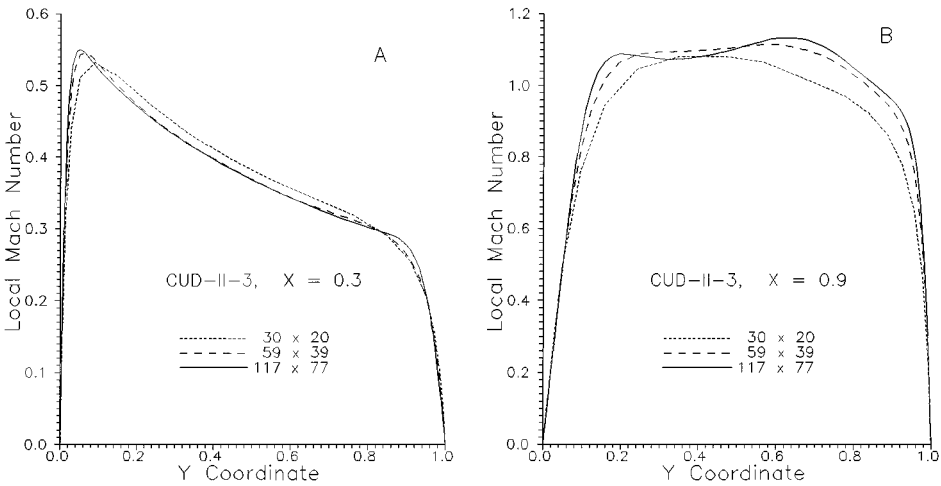

FIG. 10. Mach number distributions along $x = \text{const}$ for different meshes CUD-II-3.

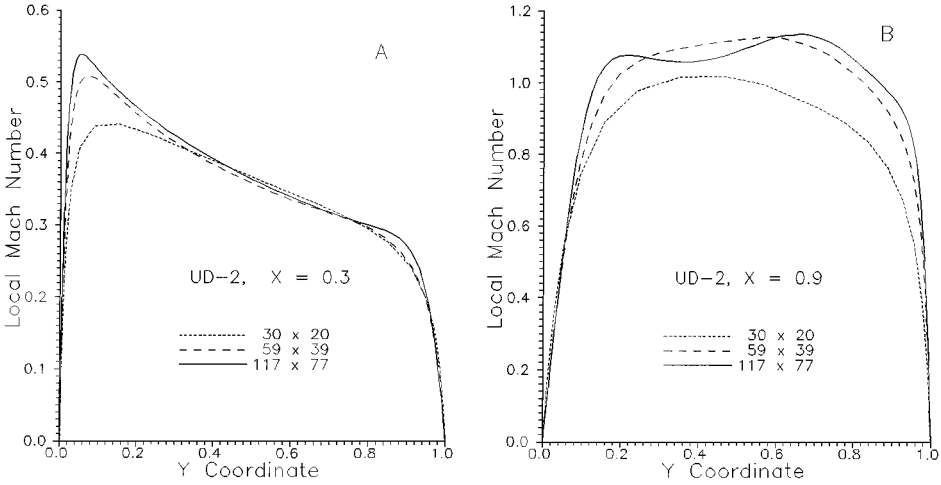

FIG. 11. Mach number distributions along $x = \text{const}$ for different meshes UD-2.

summation is performed over the grid points common to all meshes (that is, over 30×20 mesh grid points). Based on these deviations, the convergence orders were calculated as

$$\text{order}_j = \log_2 \frac{\text{err}_j}{\text{err}_{j-1}}.$$

The deviations and the orders estimated in such a way are shown in Table 4.

As can be seen, the real convergence order for all considered schemes is approximately one-half that for their inviscid term discretizations. One can observe also that the CUD-II-5 error for the 59×39 grid is about one-half the UD-2 error for the 117×77 mesh.

To estimate the dissipation introduced by the schemes in the inviscid portion of the flow, it is convenient to calculate the pressure losses defined as

$$1 - p_0'/p_0,$$

where p_0 is the total pressure at the inflow and p_0' is the total pressure computed on the basis of local flow variables using the adiabatic formula.

The pressure losses in the same cross sections, $x = 0.3$ and $x = 0.9$, are presented in Figs. 12 and 13 for CUD-II-5 and CUD-II-3, respectively. As can be seen, they are negligible outside the boundary layers, when 59×39 and 117×77 meshes are used for the CUD-II-5

TABLE 4

	UD-2		CUD-II-3		CUD-II-5	
Mesh	Err	Order	Err	Order	Err	Order
30×20	0.0762		0.0714		0.0316	
59×39	0.0372	1.03	0.0257	1.47	0.00849	2.31
117×77	0.0159	1.23	0.00789	1.70	0	

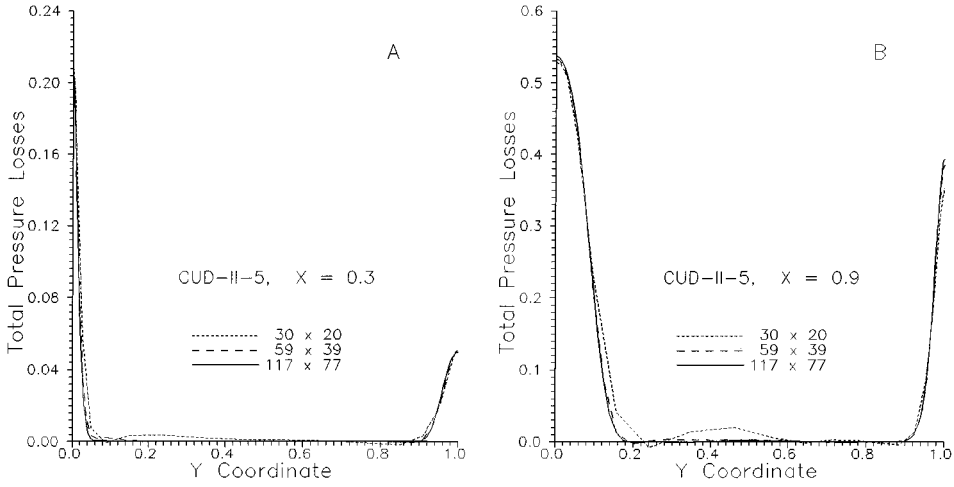

FIG. 12. Pressure losses in cross sections $x = \text{const}$ for different meshes CUD-II-5.

calculations. The values 0.01–0.02 seen in Fig. 12 for the 30×20 mesh correspond to slight Mach number deviations from the mesh-independent values (see Fig. 9).

The pressure losses calculated for UD-2 solutions (Fig. 14) show that the spurious dissipation introduced by the scheme is not negligible, even if the finest mesh is used. For coarser meshes, its values are quite pronounced.

Returning to Fig. 8a, it is possible to see a slight pressure undershoot near the trailing edge. Close examination of this region shows the fine structure of the separated flow. The ability of the fifth- and second-order schemes to resolve this structure is illustrated in Fig. 15, where streamlines near the trailing edge are presented for different meshes. Note that the "efficient" contour of the edge is also mesh-dependent.

It should be noted also that the wiggles seen in Fig. 15 are entirely due to the postprocessing of small velocity fields. These velocities were found to be smooth grid functions.

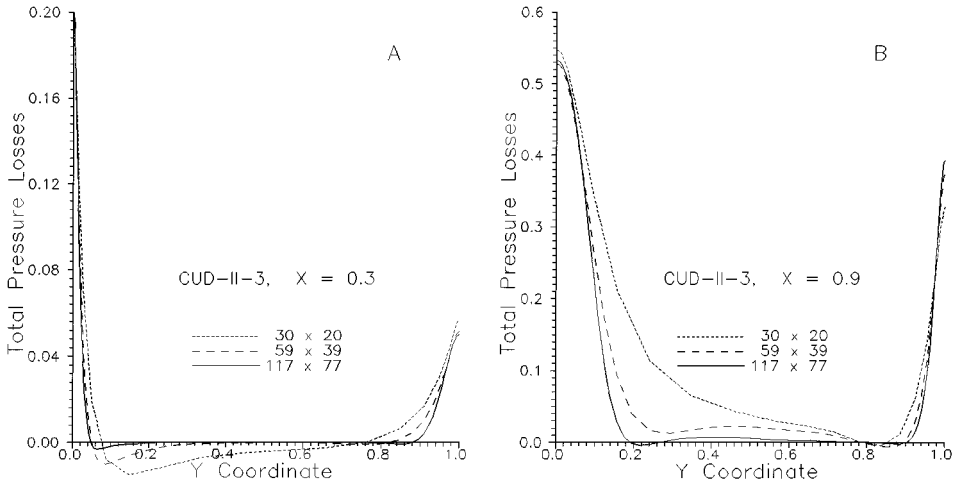

FIG. 13. Pressure losses in cross sections $x = \text{const}$ for different meshes CUD-II-3.

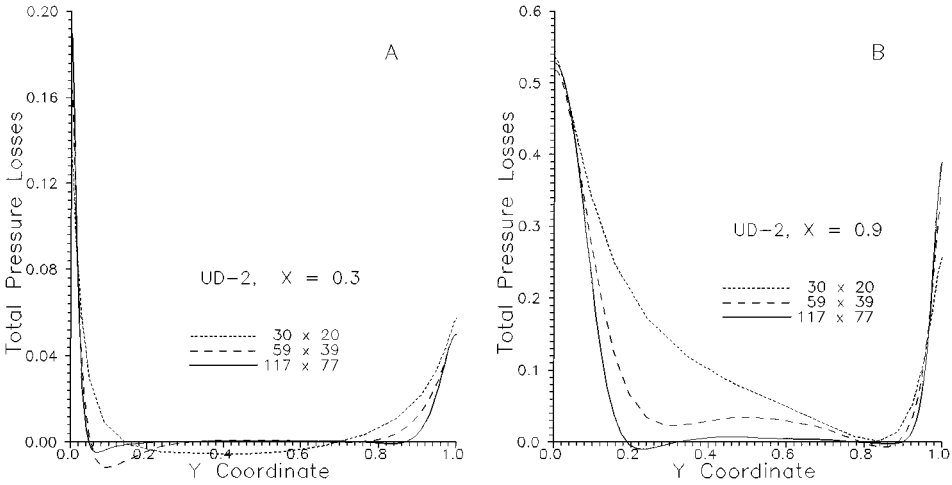

FIG. 14. Pressure losses in cross sections $x = \text{const}$ for different meshes UD-2.

As follows from the figures, the CUD-based scheme "feels" this subtle detail, even when a very coarse mesh is used. In this case, the UD-2 scheme gives a nonseparated flow pattern. When the mesh is refined (mesh 59×39), a small separation bubble is seen in the flow field, corresponding to the CUD-II-5 calculations. For this mesh, only the onset of the recirculation pattern can be noticed when inspecting the UD-2 streamlines. Closer resemblance of the flow structures is seen only for the finest mesh, the difference being due mainly to the resolution of two separation bubbles in the case of CUD-II-5.

Table 5 provides the computational costs when using an IBM PC-type computer with a Pentium 150 Mhz processor. They are evaluated on the CPU time basis and the number of steps needed to reach steady-state solutions for the 30×20 mesh when starting from a very coarse initial guess (more precisely, to reduce the initial residuals by a factor of 10^{-5}).

The quite unexpected result in Table 5 is that the CUD-II-3 calculations are cheaper than their UD-2 counterparts for a fixed mesh. The CUD-II-5 calculations when compared with those for UD-2 are more expensive approximately by a factor of 1.5. However, when the comparisons are made on the equal accuracy basis, the advantages of CUD-II-5 are evident. For example, comparing 117×77 UD-2 and 59×39 CUD-II-5 calculations (nearly mesh-converged cases), the CPU time per time step can be estimated approximately as 1.47 s and 0.528 s, respectively. Moreover, the number of time steps in the latter case was found to be less than one-third that in the former case. This fact is quite understandable due to the reduced number of grid points generating the CUD algebraic system. Therefore, the computational cost decreases roughly by a factor of 10.

TABLE 5

Scheme	CPU/step/node (sec)	Number of steps	Total CPU time (s)
UD-2	1.53×10^{-4}	4550	418.6
CUD-II-3	1.93×10^{-4}	3090	358.4
CUD-II-5	2.20×10^{-4}	4910	648.1

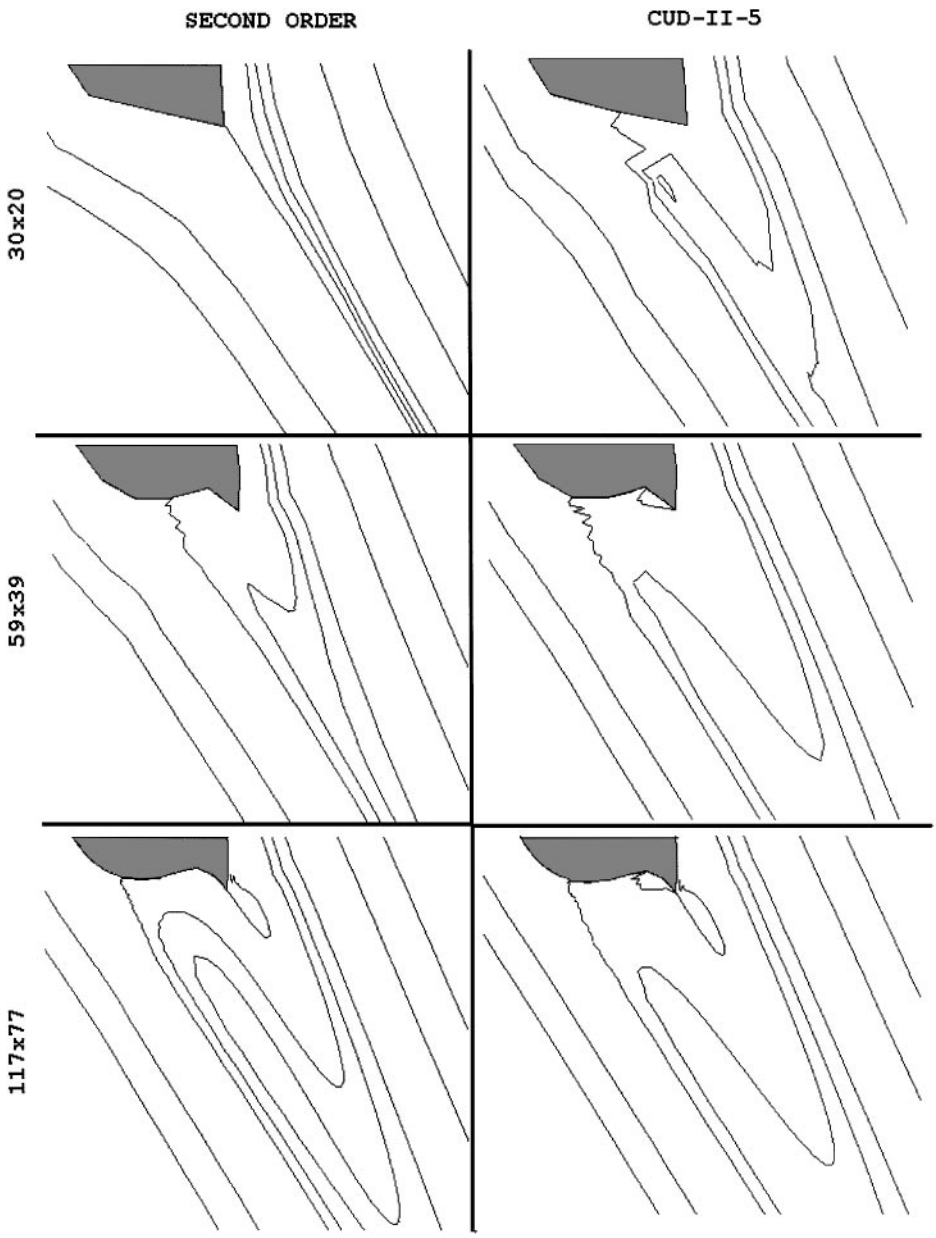

FIG. 15. Streamlines near the trailing edge: comparison of CUD-II-5 and UD-2 results.

It should be emphasized that all the above estimates are obtained without optimizing the convergence process. The "equal conditions" principle of the scheme competitions was used; that is, only inviscid approximation blocks were changed in the computer code. Of course, the total number of time steps in both cases can be reduced by some acceleration procedure with possible changes of their ratio.

The comparisons presented in Figs. 8–15 and Tables 4–5 show that, under conditions adversely affecting the accuracy (second-order discretization of the viscous terms and highly curved nonorthogonal coordinates) the CUD (especially, the fifth-order CUD) techniques

can operate with reasonable accuracy while using relatively coarse meshes. When compared with the second-order scheme, they can provide considerable savings of the operation counts for a given accuracy despite the greater operation counts per time step.

Another observation which follows from close examination of the numerical flow fields is that the solutions are absolutely wiggle-free although no artificial smoothing devices were used in the present calculations.

7. CONCLUSIONS

In the present study, recent versions of third- and fifth-order approximations are investigated. Properties of these approximations are described, the main of them being high accuracy, a "built-in" filter of spurious oscillations, and favorable response of steady-state solutions to the cell Reynolds number variation.

When constructing implicit difference schemes with CUD operators, two important elements are suggested: (i) the simple form of flux splitting, preserving both the positivity of the approximations and the conservativity of schemes in the case of vector conservation laws and (ii) the architecture of the implicit part of the algorithms with first-order upwind operators. Element (ii) and third-order CUD go well together, resulting in the method which provides rapid convergence to steady-state solutions.

The CUD schemes were tested against the inviscid and viscous Burgers equations. In the inviscid case, considerable increase of accuracy was demonstrated when calculating smooth solutions. When supplied by flux limiters, the CUD schemes are shown to have the potential for serving as parts of high-resolution schemes for discontinuous solutions.

In the viscous case, the main emphasis was placed on the study of mesh-convergence and accuracy of steady-state solutions. With a proper choice of the forcing term and boundary conditions, the exact solution consists of "inviscid" exponential parts separated by the shock-type structure. Calculations were carried out using third- and fifth-order CUD, combined with nth-order discretizations of the viscous term, $n = 2, 4, 6$. The conventional second-order differencing was also tried for comparison purposes.

The main conclusions are as follows:

(i) No limiters were needed in the present study to obtain wiggle-free steady-state solutions with steep gradients.

(ii) The fifth-order CUD provides the least L_2-errors for all uniform meshes and the viscous term discretizations used in the calculations. When the shock is properly resolved, that is, when its region contains three or more grid points, then the increase of accuracy as compared with that for the second-order scheme is measured by orders of magnitude. The accuracy is especially high when the viscous term is discretized using high-order formulae.

(iii) The order of mesh convergence depends on the dominance of TE^m_{inv} or TE^n_{vis}, the mth and nth order local truncation errors of the "inviscid" and "viscous" operators, respectively. It is close to m or n if $TE^m_{\text{inv}} >> TE^n_{\text{vis}}$ or $TE^m_{\text{inv}} << TE^n_{\text{vis}}$. In particular, the CUD-II-5 solutions show the convergence orders near 2, 4, and 5 for $n = 2, 4$, and 6.

(iv) In the underresolved case when only 1–2 grid points can be found in the shock region, all tested schemes give approximately the same order of actual accuracy. However, the usual procedure of clustering grid points in the steep gradient regions can restore the considerable advantages of CUD-II-5.

The CUD algorithms for model equations are extended to the case of the Navier–Stokes equations written in the conservative form in curvilinear coordinates. In this case, rapid variations of metric coefficients near the leading and trailing edges, skewed coordinate lines, and the high aspect ratio of the computational cell are expected to adversely affect the solution accuracy. The calculations performed using the combination "CUD & second-order discretization of viscous terms" and low-order upwind schemes show that despite the above negative factors, the CUD-based schemes provide solutions which are considerably closer to the mesh-converged result than those for the second-order method. Again, the scheme with CUD-II-5 was found to be the most accurate. Even when using very coarse 30×20 mesh, the scheme is capable of "feeling" the fine structure of the separated flow near the trailing edge, while the second-order scheme gives a nonseparated flow pattern.

As in the case of Burgers equation, the higher accuracy of the fifth-order method despite the second-order discretization of viscous terms can be explained by the relatively small truncation errors in the inviscid core of the flow which can be expected to be $\max(TE^5_{\text{inv}}, Re^{-1}TE^2_{\text{vis}})$, in contrast to TE^2_{inv} in the case of the second-order scheme. It seems to be important also that in the present steep-gradients case no smoothing techniques which can result in locally low-order truncation errors were used to obtain nonoscillating solutions.

Summing up the theoretical issues relevant to the CUD-II-3 and CUD-II-5, some understanding of their performance follows, not only from the general theory which relates to approximation and mesh-convergence orders, but also from:

(i) the general property of both centered and noncentered high-order compact discretizations characterized by small numerical constants in their truncation errors;

(ii) the specific property of compact upwind discretizations manifested in relatively well-conditioned systems of steady-state difference equations;

(iii) the specific feature of the CUD-II-3 and CUD-II-5 schemes allowing efficient preconditioning.

In the CFD area, their application seems to be especially beneficial when good resolutions (including fine details) of high Reynolds number flows with modest computational expenses is desirable. However, in the cases of relatively small Reynolds numbers and/or smooth behavior of solutions, centered compact approximations [13] may be recommended due to their accuracy and simplicity.

Concluding the discussion, we note that CUD-II-3 and CUD-II-5 possess other remarkable properties which are beyond the scope of the present paper. It turns out that their linear combinations can be used when constructing arbitrary-order schemes for parallel calculations [18]. Another interesting feature of CUD-II-5 is its ability to provide negligible phase errors practically for all wave lengths supported by grids when combined with the newly proposed CUD-based fifth-order two-step time integrators [19]. Another line of their development which is in progress now is the domain decomposition CUD technique for complicated geometries.

ACKNOWLEDGMENTS

This work is supported by the Russian Fund of Basic Researches (Grant 9317598). It is also based on research which has been partly supported by United Technology Research Center and International Science Foundation (Grant JI8100). The Gauss–Zeidel routine used in the present study was developed by Dr. D. A. Shirobokov.

REFERENCES

1. A. I. Tolstykh, On a method for the numerical solution of the compressible Navier–Stokes equations over a wide range of Reynolds numbers, *Dokl. Akad. Nauk. SSSR* **210**, 48 (1973). [Engl. transl., *Sov. Phys. Dokl.* **18**, 74 (1973)]
2. A. I. Tolstykh, *Compact Difference Schemes and Their Application to Problems of Aerohydrodynamics* (Nauka, Moscow, 1990), p. 230. [Russian]
3. A. I. Tolstykh, On the non-symmetric three point difference schemes of the fourth and fifth orders, *Zh. Vychis. Mat. Mat. Fiz.* **25**, 1164 (1985). [English transl., *USSR Comput. Math. Math. Phys.* **25**, 127 (1985)]
4. V. A. Garanzha and A. I. Tolstykh, On numerical simulation of unsteady incompressible flows on the bases of fifth-order compact approximations, *Dokl. Acad. Nauk SSSR* **312**, 311 (1990). [Russian]
5. A. I. Tolstykh and K. S. Ravichandran, *Compact Upwind Difference Schemes for Scalar Conservation Laws*, NAL TM CF 9101, Bangalore, 1991.
6. K. S. Ravichandran, *CUD-3 Schemes with Runge-Kutta Time Stepping for Euler Equations*, NAL PDCF 9401, Bangalore, 1994.
7. I. F. Muzafarov, G. A. Tirskii, S. V. Utyuzhnikov, and N. K. Yamaleev, Numerical simulation of the flow over a body flying through a thermal in stratified atmosphere, *Comput. & Fluids* **23**(9), 295 (1994).
8. A. I. Tolstykh, On a class of non-centered compact difference schemes of fifth order based on Pade approximants, *Dokl. Akad. Nauk SSSR* **319**, 72 (1991). [Engl. transl., *Sov. Math. Dokl.* **44**, 69 (1992)]
9. A. I. Tolstykh, On iterative schemes with non-centered compact approximations, *Dokl. Akad. Nauk* **326**, 425 (1992).
10. A. I. Tolstykh, *High Accuracy Non-centered Compact Difference Schemes for Fluid Dynamics Applications* (World Scientific, Singapore, 1994), p. 314.
11. B. Cockburn and C. W. Shu, Nonlinearly stable compact schemes for shock calculations, *SIAM J. Numer. Anal.* **31**(3), 607 (1994).
12. N. A. Adams and K. Shariff, A high-resolution hybrid compact-ENO scheme for shock-turbulence interaction problems, *J. Comput. Phys.* **127**, 27 (1996).
13. S. K. Lele, Compact finite-difference schemes with spectral-like resolution, *J. Comput. Phys.* **103**, 16 (1992).
14. X.-D. Liu and S. Osher, Nonoscillatory high order accurate self-similar maximum principle satisfying shock capturing schemes, *SIAM J. Numer. Anal.* **33**, 760 (1996).
15. S. T. Zalesak, Fully multidimensional flux-corrected transport algorithms for fluids, *J. Comput. Phys.* **31**, 335 (1979).
16. K. S. Ravichandran, *Steady State Calculations Using Compact Upwind Schemes for the Inviscid and Viscous Burger's Equation*, NAL Tech. Memo. 9201, Bangalore, 1991.
17. Y. Saad and M. H. Shultz, GMRES: A generalized minimal residual algorithm for solving nonsymmetric linear systems, *SIAM J. Sci. Statist. Comput.* **7**, 856 (1986).
18. A. I. Tolstykh, Multiopperator high-order compact upwind methods for CFD paralell calculations, in *International Conference Parallel CFD'97, Manchester, England, May 19–21, 1997.* [Submitted for publication]
19. A. I. Tolstykh, Fifth-order two-step time integrators with applications to PDEs and stiff ODEs, in *Proceedings, 15th IMACS World Congress on Scientific Computation, Modelling and Applied Mathematics, Berlin, August 1997* (Wissenshaft & Technik Verlag, Berlin, 1997), Vol. 2, p. 39.